Report

Cell Reports

Axon Dynamics during Neocortical Laminar Innervation

Graphical Abstract

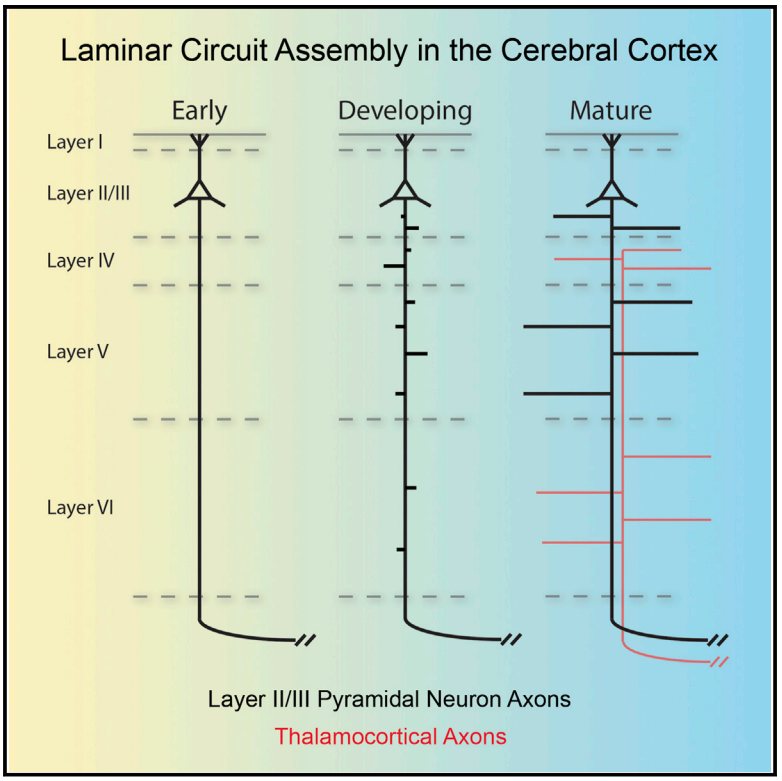

Authors

Randal A. Hand, Syed Khalid, Edric Tam, Alex L. Kolodkin

Correspondence

kolodkin@jhmi.edu

In Brief

The cerebral cortex is a laminated, highly interconnected structure. Hand et al. use live imaging to examine cell dynamics underlying initial laminar-specific innervation of the cerebral cortex by layer II/III pyramidal neurons. They find that axon collateral branches are selectively stabilized in target laminae.

Highlights

- Axons are highly dynamic during laminar innervation
- Axon collateral branches are selectively stabilized in target laminae
- F-actin pools are predictive of axonal protrusions
- Neuronal activity is dispensable for local somatosensory cortex innervation

Hand et al., 2015, Cell Reports *12*, 172–182
July 14, 2015
http://dx.doi.org/10.1016/j.celrep.2015.06.026

OPEN ACCESS
CellPress

Cell Reports
Report

Axon Dynamics during Neocortical Laminar Innervation

Randal A. Hand,[1] Syed Khalid,[1] Edric Tam,[1] and Alex L. Kolodkin[1,*]
[1]The Solomon H. Snyder Department of Neuroscience and Howard Hughes Medical Institute, The Johns Hopkins University School of Medicine, Baltimore, MD 21205, USA
*Correspondence: kolodkin@jhmi.edu
http://dx.doi.org/10.1016/j.celrep.2015.06.026

SUMMARY

The cerebral cortex is a densely interconnected structure with neural circuits that form between cortical laminae and also between distinct cortical areas. However, the precise cell biological and developmental mechanisms that underlie the formation of these neural circuits remain unknown. Here, we visualize laminar innervation of the developing mouse cerebral cortex by layer II/III pyramidal neurons in real time, describing cytoskeletal dynamics during this process. We find that layer II/III pyramidal neurons achieve local laminar-specific innervation through the stabilization of collateral axon branches in target laminae. We also find that loss of neural activity does not abolish local laminar-specific innervation and that cells within the local environment are the likely source of cues that direct layer-specific cortical innervation.

INTRODUCTION

The neocortex is the largest region of the cerebral cortex and is organized into functional regions, or areas, that typically contain six discrete laminae. Pyramidal neurons from layers II and III (referred to as ''layer II/III'') are similar, and their axons constitute most of the callosal tract (Fame et al., 2011). Layer II/III pyramidal neurons exhibit dense innervation of layers II/III and V locally within their resident cortical area (Figures 1A–1C), within their long-range contralateral cortical target areas, and also in other distinct ipsilateral cortical areas (Figure S1A). The mechanisms that regulate laminar-specific innervation within the cerebral cortex are enigmatic; however, axonal branching is a necessary step in this process. Axon branching is critical for establishing connectivity in most neural systems, and signaling pathways and cytoskeletal rearrangements that underlie axon branching have been investigated in vitro (Dent et al., 1999; Dent and Kalil, 2001; Kalil and Dent, 2014). Several types of axon branching are important for generating cerebral cortex innervation patterns, including bifurcations, the splitting of a growing axon at the growth cone; terminal arborizations, which occur at the distal end of axons and consist of dense higher order branches; and collateral axon branches, processes that emerge orthogonally from the main axonal projection distant from the axon terminal (Gibson and Ma, 2011).

Here, we investigate the cell dynamics and developmental mechanisms underlying local laminar innervation exhibited by neocortical layer II/III pyramidal neurons. We visualize the formation of collateral axon branches within the developing cerebral cortex, utilizing in-depth real-time analysis of collateral branch formation to reveal the establishment of local cerebral cortical laminar-specific innervation. Further, we investigate cytoskeletal dynamics during this process and explore potential sources of cues that direct local laminar-specific innervation of the layer II/III pyramidal neurons. This work provides an important first step toward identifying developmental and molecular mechanisms underlying local laminar-specific innervation within the cerebral cortex.

RESULTS

Laminar-Specific Innervation of Cortical Areas by Layer II/III Pyramidal Neurons

To understand how layer II/III pyramidal neurons in primary somatosensory cortex (S1) form discrete circuits in select cortical layers, we performed an axon innervation developmental time course. We labeled S1 layer II/III pyramidal neurons using targeted in utero electroporation (IUE) in embryonic day 15.5 (E15.5) mouse embryos with plasmids encoding eGFP. Electroporated embryos were born and then analyzed at various postnatal time points for laminar and areal innervation patterns (Figure S1).

The initial projections from these primary axons form and project toward the corpus callosum prior to the initiation of radial migration, before pyramidal neurons reach the cortical plate (Hand and Polleux, 2011; Hatanaka and Yamauchi, 2013). These axons approach the CNS midline around postnatal day 0 (P0) (Figure S1B) and cross it by P3. We first observed innervation locally in ipsilateral S1 at P3. This occurred through collateral axon branch formation in layer V (Figure S1C), and we noted widespread branch formation by P5 (Figure S1D). Formation of an axonal plexus in layer V by labeled layer II/III neurons is observed at P10, and dense layer V innervation is seen at P14 (Figures S1E and S1F). In addition to innervating local ipsilateral S1, S1 layer II/III pyramidal neurons innervate distant targets including contralateral S1, ipsilateral primary motor cortex (M1),

and ipsilateral secondary somatosensory cortex (S2) (Akers and Killackey, 1978), forming terminal arbors and laminar-specific innervation of layers II/III and V (Figures S1G–S1N; Table S1).

Dynamics of Layer II/III Collateral Axon Branch Formation

We next sought to understand the cell dynamics underlying local laminar innervation. We examined individual neurons using a sparse labeling approach, and at P0, we found that the primary axon projected toward the corpus callosum and did not extend collateral axon branches (Figures 1D and 1G). By P5, many collateral axon branches had emerged from the primary axon (Figures 1E and 1H), and at P21, the highly stereotyped innervation pattern of S1 layer II/III pyramidal neurons was apparent (Figures 1F and 1I). P3 was the earliest time point when we observed collateral axon branches extending from S1 layer II/III pyramidal neurons (Figures 1J and 1K). In addition to collateral axon branches, we also observed many small protrusions along primary axon shafts (Figures 1L and 1M).

How is local laminar-specific innervation established by S1 layer II/III pyramidal neurons? Are collateral axon branches formed only in target lamina, or are they formed in all lamina and refined to achieve appropriate laminar-specific targeting? We addressed these issues by visualizing local laminar-specific innervation by S1 layer II/III pyramidal neuron axons in vivo. To assess S1 layer II/III pyramidal neuron axon dynamics during neonatal development, we imaged live organotypic brain sections labeled by IUE (Figure 2A; Movie S1). Imaging began at P2.5, just prior to the initiation of layer II/III pyramidal neuron collateral axon branch formation, and sparse labeling permitted tracking of individual axons and their emerging collateral axon branches (Figure 2B). We defined collateral axon branches as lamellipodium-like protrusions with an axon-like shaft that extend for at least 6 μm from the primary axon. We found that, although collateral axon branches emerged across all cortical layers (Figures 2C and 2D), layer V had the highest rate of collateral branch formation (Figure 2E), a significantly higher branch formation rate than layers II/III or VI ($p = 0.0100$ and $p = 0.0188$, respectively) on average more than twice that of layer IV ($p = 0.0782$; Figure 2E). When we normalized the branch rate to a unit axon length (branches per hour per 100 μm of axon), we found similar branch formation rates among layers II/III, IV, and V (Figure 2F).

We next asked whether there is a difference in collateral axon branches formed in different cortical layers. Although collateral axon branches were initiated across all cortical layers (Figure 2D), the most dramatic differences in collateral axon branch dynamics were in branch length and stability within layer V. Whereas this phenomenon can be observed in sparsely labeled neurons (Movie S2), it is more easily appreciated when a large number of neurons are observed simultaneously. We employed an approach based on the multiaddressable genome-integrative color (MAGIC) markers, a plasmid-based "Brainbow" technology (Loulier et al., 2014; Figure S2; Movie S3), and quantitatively assessed layer II/III pyramidal neuron branching. We grouped the collateral axon branches from our sparse labeling time-lapse images by layer, length (<10 μm or >10 μm), and duration (<120 min or >120 min). Within layer V, we found significantly more collateral axon branches longer than 10 μm and also more branches that persisted longer than 120 min (Figures 2G and 2H). This suggests that cues within layer V support extension and stabilization of collateral axon branches. Whereas we did not observe an increase in stable collateral axon branches within layer II/III in ipsilateral S1 at P2.5–P4, we did find elongated collateral axon branches in layer II/III beyond P5 (Figures 1 and S1), suggesting a slight developmental delay in the formation of collateral axons in layer II/III. We did not observe collateral axon branches within layer IV beyond P10 (Figures 1 and S1), suggesting that cues in layer IV ultimately inhibit branch stability and innervation.

Collateral Axon Branch Formation by Pyramidal Neurons in Layers II/III

In both our fixed images (Figures 1K–1M) and our live imaging data (Figure 2B; Movies S2 and S3), we observed many small protrusions along the primary axon. Because these filopodia and lamellipodia represent initial steps in collateral axon branch formation (Kalil and Dent, 2014), we analyzed them with high spatial and temporal resolution.

In these time-lapse images, we observed 25 primary axons, spanning all cortical layers, and these axons produced 566 small filopodium-like protrusions, 36 lamellipodium-like protrusions, and 5 collateral axon branches. Filopodium-like protrusions were defined as thin protrusions (less than 2 μm in width), lamellipodium-like protrusions were defined as wider protrusions (greater than 2 μm in width), and collateral axon branches were defined as lamellipodium-like protrusions with an axon-like shaft that extend at least 6 μm from the primary axon. Both the initiation and retraction of these protrusions were observed along the entire length of the axon shaft (Figure 3A; Movie S4). When we compared the average rate of filopodium formation across cortical layers, we found a significant increase in upper cortical layers (II–IV) compared to deeper layers (layers V and VI; Figure 3B). Further, we did not observe any significant differences in filopodium length or persistence across cortical layers (Figures 3C and 3D). We found a significant difference in lamellipodium formation rates only between layers II/III and VI (Figure 3E), and we did not observe any difference in the length or persistence of lamellipodia among layers II/III, IV, or V (Figures 3F and 3G; we did not observe sufficient numbers of lamellipodia in layer VI to make a comparison). Interestingly, the rate of collateral axon branch formation did not correspond to either the rate of filopodium formation nor lamellipodium formation across cortical layers (Figures 2E, 2F, 3B, and 3E). Our data demonstrate that layer II/III primary axons within ipsilateral S1 are highly dynamic, with many small filopodium-like and lamellipodium-like protrusions occurring along the entire length of their axon shafts.

F-Actin Dynamics along the Primary Axon

Because the actin cytoskeleton underlies the formation of filopodium and lamellipodium-like protrusions (Kalil and Dent, 2014), we employed a fluorescent f-actin biosensor to better understand actin cytoskeletal dynamics within them. The calponin homology domain of the f-actin-binding protein utrophin fused to mRFP (mRFP-UtrCH) binds f-actin with high affinity and serves as an f-actin reporter in living cells (Burkel et al., 2007).

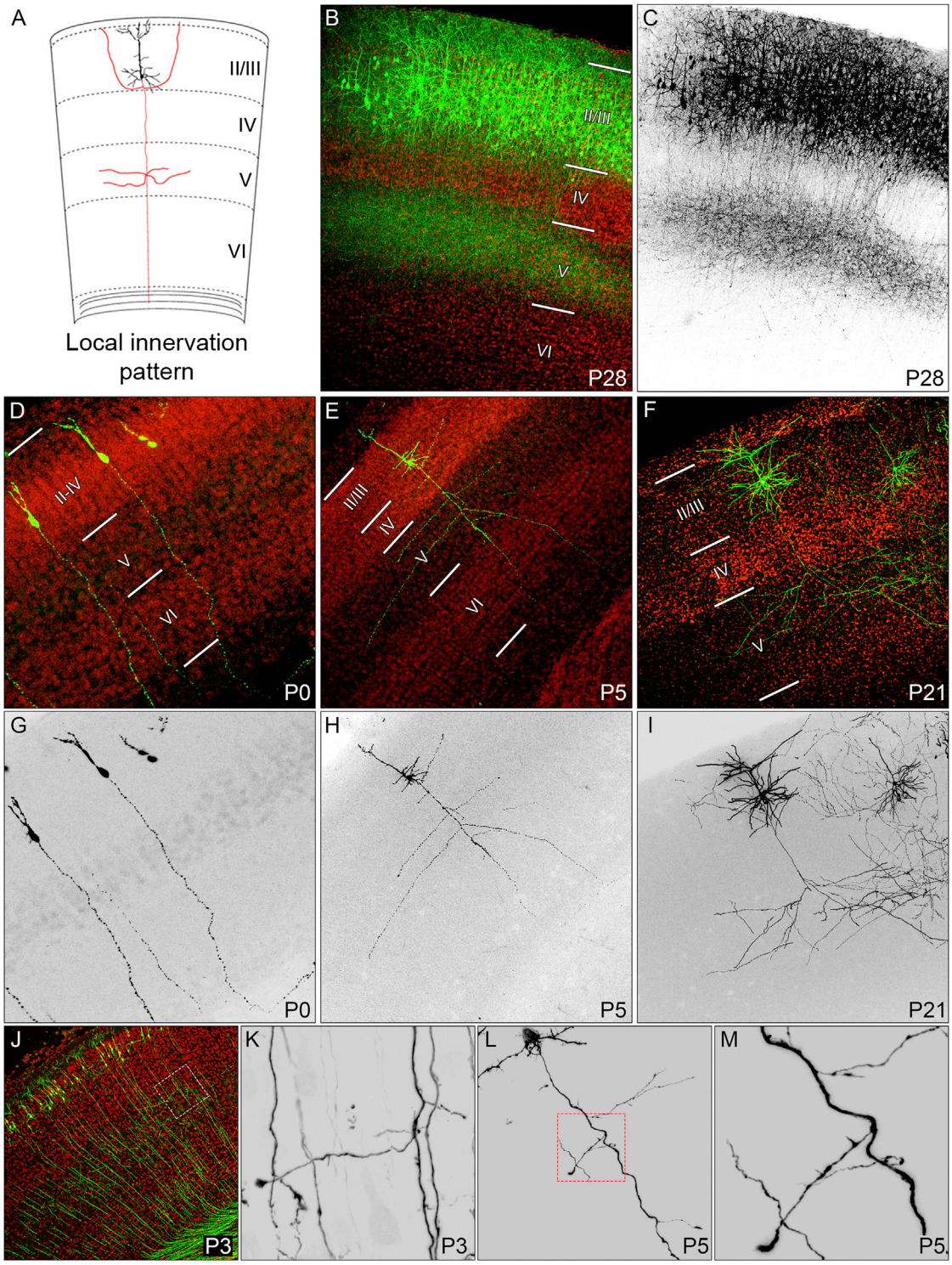

Figure 1. Visualization of Local Collateral Axon Branch Formation in Ipsilateral S1

(A) A schematic diagram illustrating the local innervation pattern of layer II/III pyramidal neurons in S1.

(B and C) The final local innervation pattern of S1 layer II/III pyramidal neurons observed at P28 by introducing constitutive eGFP expression plasmids into layer II/III pyramidal neurons by IUE (green: B; black: C).

(legend continued on next page)

We sparsely labeled axons using plasmids encoding mRFP-UtrCH and eGFP by IUE to simultaneously visualize axons (eGFP fluorescence) and f-actin (mRFP fluorescence) in layer II/III pyramidal neuron axons (Figure 4A; Movie S5). In addition to f-actin within filopodia, lamellipodia, and axon growth cones, we also observed f-actin pools along the axon shaft. Whereas the precise role of these f-actin pools is unclear, they may be important for initiating protrusions from the axon shaft.

We analyzed 647 f-actin pools from our time-lapse images, focusing on f-actin pools located in layers II/III, IV, and V, cortical layers containing the highest rate of filopodia and lamellipodia formation (Figures 3B and 3E). The f-actin pools we quantified were at least 0.25 μm^2 in area, a size we could reliably detect and track in our images. When we binned these f-actin pools by area, we found that 30.45% of the f-actin pools had an area between 0.25 μm^2 and 0.49 μm^2, 32.30% had an area between 0.5 μm^2 and 0.99 μm^2, 20% had an area between 1.0 μm^2 and 1.99 μm^2, and 16.38% had an area greater than 2.0 μm^2 (Figure 4B). We also assessed the duration of each f-actin pool, and when we binned these f-actin pools by duration, we found that 45.3% persisted less than 2.5 min, 29.2% persisted between 2.5 and 5 min, 14.1% persisted between 5.1 and 15 min, and 11.4% persisted more than 15 min (Figure 4C). We next determined whether there was a correlation between the area and duration of f-actin pools and found that indeed there was (p value < 0.0001; Figure 4D). We also explored the relationship between f-actin pools and axon protrusions, finding that, of the 647 f-actin pools we analyzed, 417 (64.45%) were co-localized with a protrusion. The average area of an f-actin pool with a protrusion was significantly larger than the average area of an f-actin pool without a protrusion (1.539 μm^2 versus 0.634 μm^2, respectively; p value < 0.0001; Figure 4E). Similarly, we found that f-actin pools co-localized with a protrusion persisted significantly longer than f-actin pools that were not (10.74 min versus 1.88 min, respectively; p value < 0.0001; Figure 4F). We also observed a significant difference between the change in area of an f-actin pool upon loss of a protrusion compared to formation of a new protrusion (-0.078 μm^2 versus 0.163 μm^2, respectively; p value < 0.05; Figure 4G). When we compared the percentage of f-action pools co-localized with a protrusion across cortical layers, or the size and persistence of actin pools across cortical layers, we found no significant differences (data not shown).

Because we observed a difference in the area of an f-actin pool co-localized with a protrusion as compared to those that were not (Figure 4E), we sought to assess the predictive value of the area of an f-actin pool with respect to protrusion formation. For f-actin pools with areas between 0.25 μm^2 and 0.49 μm^2, there was no significant difference in the percentage of pools that either did, or did not, correspond to a protrusion. However, for f-actin pool with larger areas, a significant proportion is associated with a protrusion (Figure 4H). When we binned f-actin pools by duration, we found an equal proportion of f-actin pools that either did, or did not, correspond to a protrusion persisted for the least amount of time we scored (less than 2.5 min). However, as the duration of f-actin pools increased, a significantly higher proportion correlated with a protrusion (Figure 4I). These results, taken together, suggest that smaller and more-transient f-actin pools do not necessarily correspond with a protrusion extending from the primary axon, but as the size and persistence of an f-actin pool increase, it is highly likely to be associated with the formation of a protrusion.

Midline Crossing, Callosal Axons, and Thalamocortical Axons Are Dispensable for Laminar Innervation by Pyramidal Neurons in Layers II/III

Cytoskeletal actin and microtubules regulate axonal morphology in response to extrinsic cues. However, the sources of extrinsic cues that direct layer II/III pyramidal neuron laminar-specific innervation patterns in layers II/III are unknown. Because these axons cross the CNS midline prior to undergoing ipsilateral collateral axon branching, it is possible that a midline extrinsic instructive factor acts retrogradely to induce collateral branch formation or that an instructive cue is presented by callosal axons from the contralateral hemisphere. To test whether midline crossing or callosal axons from the contralateral hemisphere are required for initiation of collateral axon branching or for correct local laminar innervation by ipsilateral S1 layer II/III pyramidal neurons, we labeled these neurons by IUE with plasmids encoding eGFP and then lesioned the corpus callosum with a microscalpel at P0. At P0, axons from layer II/III neurons in S1 are approaching the midline but have yet to cross (Figure S1B). When we compared innervation and branching patterns in the ipsilateral S1 between control and lesioned animals, we observed no major differences (Figures 5A–5F). Quantitative assessment of layer II/III pyramidal neuron innervation was calculated for each sample by determining the ratio of immunofluorescence within each layer to the total fluorescence in all cortical layers, thereby normalizing for any variance in the number of labeled neurons. This revealed significantly more axon branches and innervation within layer V relative to layers IV and VI in both control and lesioned animals (Figure 5G; the fluorescent signal in layers II/III also includes dendrites and cell bodies, so we did not include layer II/III in this analysis).

Callosal axons are not the only afferent projections that innervate S1 in a laminar-specific fashion. During early postnatal development, thalamocortical axons (TCAs) form dense arbors in layers IV and VI (Price et al., 2006), a pattern complimentary to that of layer II/III pyramidal neuron innervation of layers II/III and V in S1 (Figures S3A–S3D). Because TCAs could present an instructive cue to direct local laminar innervation by layer II/III pyramidal neurons, we transected TCAs at P0, before they could establish their laminar-specific innervation pattern. To be certain our TCA lesions were effective, we labeled TCA axons by

(D–M) Cortical layers were determined by counterstaining with the nuclear stain DAPI (red: B, D–F, and J). Layer II/III pyramidal neurons were sparsely labeled with eGFP expression plasmids (green: D–F and J; black: G–I and K–M) by IUE. Low-magnification images of ipsilateral S1 were taken at P0 (D and G), P3 (J), P5 (E and H), and P21 (F and I). High-magnification images of primary axons at P3 reveal the emergence of collateral axon branches in layer V (white box: J and K). By P5, collateral axon branches were observed in upper cortical layers (E, H, and L; high magnification; red box: L and M).
See also Figure S1.

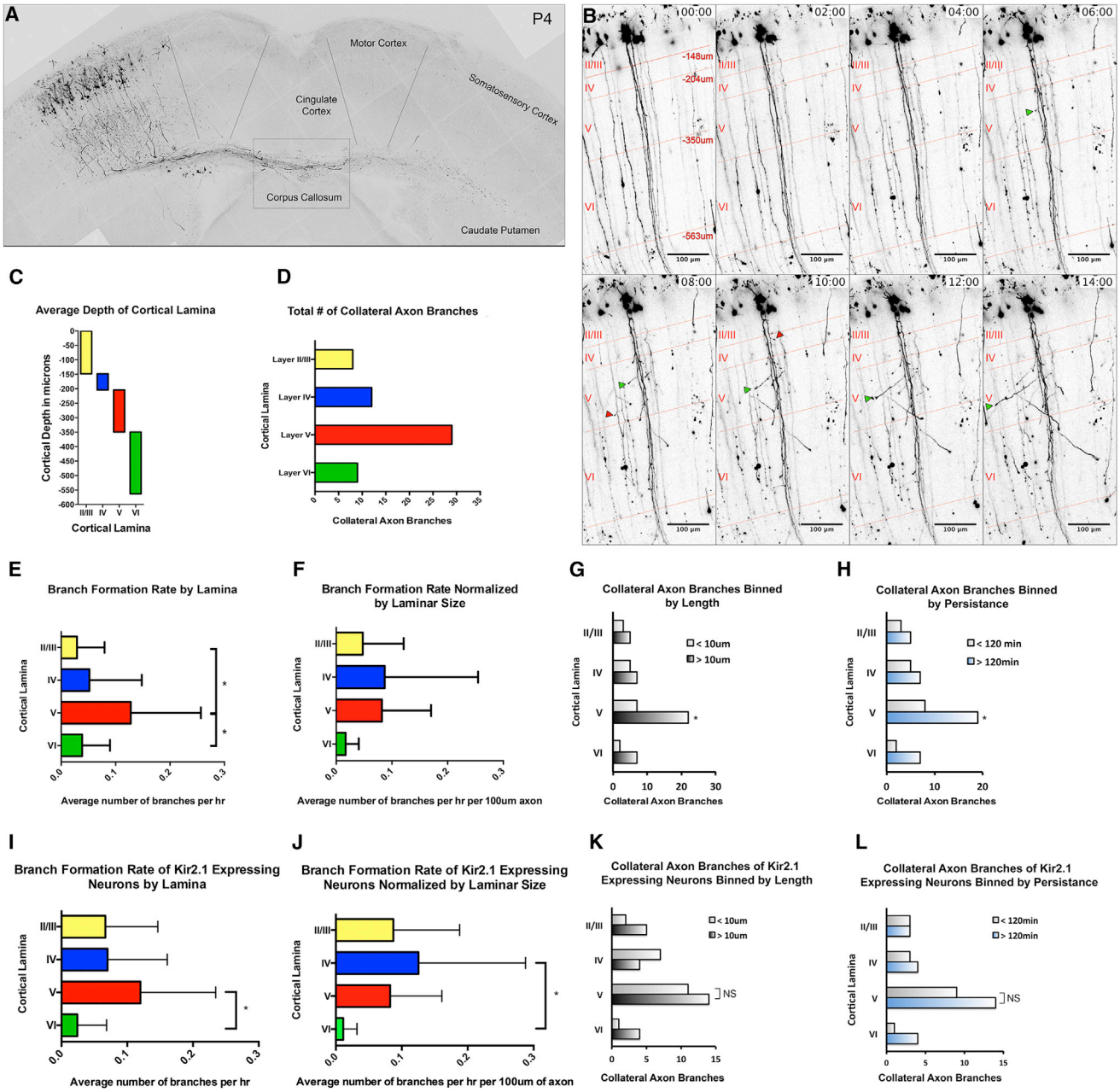

Figure 2. Real-Time Analysis of Collateral Axon Branch Formation by Layer II/III Pyramidal Neurons in S1

(A) A single image from a time-lapse imaging session obtained from an organotypic brain slice (see also Movie S1).

(B) Representative time-lapse images of layer II/III pyramidal neurons between P2.5 and 3.5 (see also Movie S2). Red lines and cortical layer labels demarcate average depth of cortical layers. At P3, layer II/III spans a depth of −148 μm, layer IV spans a depth between −148 μm and −204 μm, layer V spans a depth between −204 μm and −350 μm, and layer VI spans a depth between −350 μm and −562 μm. We found both short, transient, collateral axon branches (red arrows) and longer, more-stable, collateral axon branches (green arrows) emerging from primary axons.

(C) Graphical representation of average cortical depth by lamina.

(D) Total number of collateral axon branches formed in each lamina during our imaging sessions.

(E and F) The average branch formation rate was determined within each lamina in its entirety (E) and for each lamina by unit length of axon (F). To assess any difference in collateral axon branches formed in each lamina, a categorical analysis of axon branches was performed.

(G and H) Collateral axons were grouped by layer and length (G) and by persistence (H). Spontaneous activity contributions to the formation of collateral axon branches were determined with an analysis of time-lapse images of Kir2.1-expressing neurons.

(I and J) The average rate of branch formation was determined within each lamina in its entirety (I) and for each lamina by unit length of axon (J) of Kir2.1-expressing neurons.

(legend continued on next page)

injecting AAV8-encoding eGFP into the thalamus just prior to lesioning at P0. Our TCA lesions transected the cortical wall, extending from the prefrontal cortex through the visual cortex, across the entire extent of S1 (Figure S3F). Lesioned mice were sacrificed at P14 to allow for sufficient expression of AAV-encoded eGFP and to test whether or not TCAs were able to regrow across the lesion site (Figures S3G and S3H). After confirming the effectiveness of our TCA lesions, we next performed TCA lesions on mice in which layer II/III pyramidal neurons were first labeled by IUE with plasmids allowing for sparse and robust tdTomato expression. We observed no apparent alterations in local ipsilateral S1 laminar innervation patterns in lesioned animals as compared to controls at P5, the earliest time point at which we can observe laminar-specific innervation by S1 layer II/III pyramidal neurons (Figures 5H–5N). This suggests that TCAs are not required in vivo for the ipsilateral S1 layer II/III pyramidal neuron local laminar-specific innervation patterns. Taken together, our lesioning results suggest that cues regulating layer II/III laminar-specific innervation of the ipsilateral S1 are presented by cells residing locally within the target area.

Spontaneous Neural Activity Is Not Necessary for Layer II/III Pyramidal Neuron Laminar-Specific Innervation of the Ipsilateral S1

Neural activity in layer II/III pyramidal neurons is necessary for proper terminal arborization in the contralateral cortex (Mizuno et al., 2007, 2010; Suárez et al., 2014; Wang et al., 2007). To test whether modulating the activity of these neurons affects their laminar-specific innervation in ipsilateral S1, we dampened intrinsic neural activity by hyperpolarizing layer II/III pyramidal neurons. The expression of Kir2.1, an inwardly rectifying potassium channel, is effective in chronically modulating intrinsic activity of neurons in many different systems, including layer II/III pyramidal neurons (Bortone and Polleux, 2009; De Marco García et al., 2011; Johns et al., 1999; Mizuno et al., 2007; Suárez et al., 2014; Yu et al., 2004). We performed live imaging of Kir2.1-expressing S1 layer II/III pyramidal neurons and determined collateral axon branch formation rates across all cortical layers in their entirety, finding that it was highest in layer V (Figure 2I). However, when we compared branch formation rates across layers normalized for laminar depth in Kir2.1-expressing neurons, only the difference in branch formation rates between layer IV and layer VI was significant (Figure 2J). We also compared the branch formation rates between control neurons and Kir2.1-expressing neurons (Figures 2E and 2F versus 2I and 2J, respectively) by two-way ANOVA and found no significant difference in branch formation rates between control neurons and Kir2.1-expressing neurons (data not shown). To better understand Kir2.1 effects on collateral axon branch dynamics, we categorized these branches by layer, length, and duration. We found a significant increase in the number of collateral axon branches within layer V that were greater than 10 μm in length and also an increase in the number of axon branches that persisted longer than 120 min, as compared to layers II/III and VI (but not layer IV; Figures 2K and 2L). These results from layer II/III pyramidal neurons expressing Kir2.1 are similar to neurons expressing only eGFP: a higher rate of collateral branch formation within layer V with longer and more-persistent collateral branches. However, we do observe an increase in the number of unstable branches within layer V in Kir2.1-expressing neurons (Figures 2K and 2L) compared to neurons expressing eGFP alone (Figures 2G and 2H), suggesting that the intrinsic activity of layer II/III pyramidal reduces the formation of unstable collateral branches within layer V.

To determine whether altering neuronal activity effects the final local laminar-specific innervation patterns of S1 layer II/III pyramidal neurons, we introduced plasmids encoding tdTomato (to label neurons) along with plasmids encoding either IRES-eGFP (control) or Kir2.1-IRES-eGFP into layer II/III pyramidal neurons by IUE (Figures S4A, S4B, S4D, and S4E). We next compared the density of axons in cortical layers at early and late time points (P5 and P14, respectively) following expression of Kir2.1 in layer II/III pyramidal neurons. We found Kir2.1 expression did not alter the overall innervation pattern of layer II/III pyramidal in the ipsilateral S1 cortex. At P5 and P14, we found a significant increase in the fluorescence intensity of both eGFP and tdTomato in layer V, compared to layers IV and VI, in both control animals and in animals expressing exogenous Kir2.1 (Figures S4C and S4F). These results demonstrate that intrinsic activity alone does not dictate the laminar-specific layer II/III pyramidal neuron innervation patterns in the ipsilateral S1.

DISCUSSION

Our real-time analysis of cortical collateral axon branch formation and developmental time course reveals that collateral axon branches are formed in all cortical layers; however, they are elongated and stabilized selectively within layers II/III and V. Upon examining collateral axon branch formation dynamics, we find that the primary axon contains many dynamic f-actin-rich filopodia and lamellipodia. However, the rate of filopodium or lamellipodium formation does not correlate with the rate of axon branch formation, suggesting distinct molecular mechanisms underlie these processes. We also find that larger, more stable f-actin pools within the primary axon coincide with the formation of axon protrusions. We explored possible sources of extrinsic cues that regulate laminar innervation locally within the ipsilateral cortex and rule out contributions from the CNS midline, the contralateral cortex, and the thalamus. We also find that hyperpolarizing neurons does not abolish laminar-specific innervation in ipsilateral S1. Thus, extrinsic cues regulating the local laminar innervation by S1 layer II/III pyramidal neurons are most likely presented by cells locally within ipsilateral S1.

(K and L) A categorical analysis of the axon branches formed was performed, and collateral axon branches of Kir2.1-expressing neurons were grouped by layer by length (K) and persistence (L).

Branch formation rates were assessed by ANOVA followed by a Tukey's test (E, F, I, and J), and collateral axon branch length and persistence were analyzed using a Cochran's Q test (G, H, K, and L). * indicates a p value < 0.05. Error bars denote SD. See also Movies S1, S2, and S3.

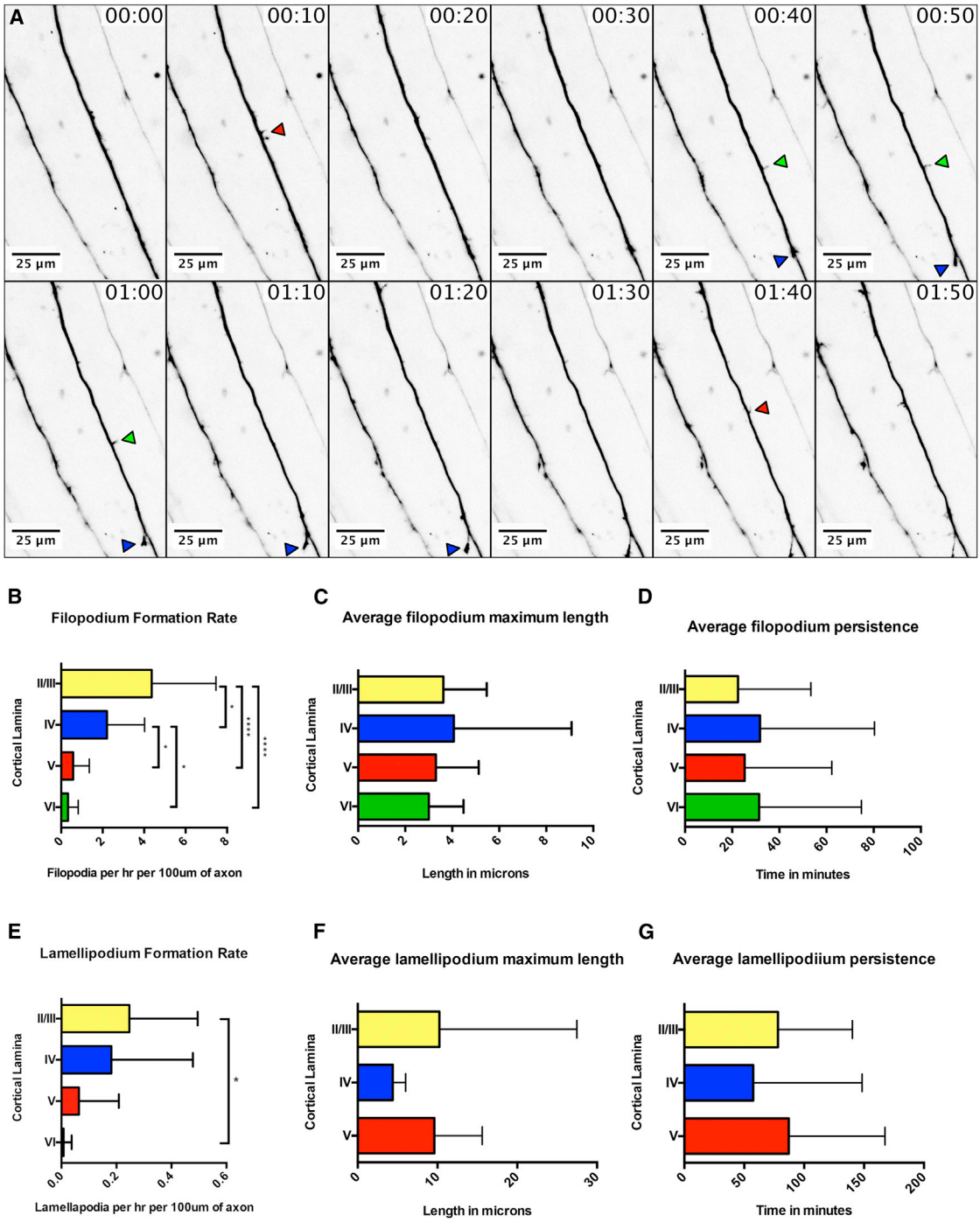

Figure 3. Real-Time Analysis of Filopodial and Lamellipodial Dynamics during Collateral Axon Branch Formation by Layer II/III Pyramidal Neurons in Ipsilateral S1

(A) Representative images from a time-lapse analysis of filopodial dynamics along primary axons from layer II/III pyramidal neurons within ipsilateral S1 (see also Movie S4). Red arrows denote transient filopodia, green arrows more-persistent filopodia, and blue arrows the successful formation of a collateral branch. (B–D) Time-lapse images were acquired in all cortical layers, and axons were assessed for filopodium formation (B), filopodium length (C), and filopodium persistence (D). Filopodia were generated in all cortical layers, with the highest rate of formation occurring in the most superficial layers (B). No significant difference was found in the average maximum length of filopodia across cortical layers (C) or in the average persistence of filopodia across cortical layers (D). (E–G) Similar to filopodia, we found that lamellipodia were generated in all cortical layers, with the highest formation rate occurring in the most superficial layers (E). We did not observe a significant difference in the average maximum length or average persistence of lamellipodia across cortical layers (F and G, respectively). * indicates a p value < 0.05, and **** indicates a p value < 0.0001. Error bars denote SD. See also Movie S4.

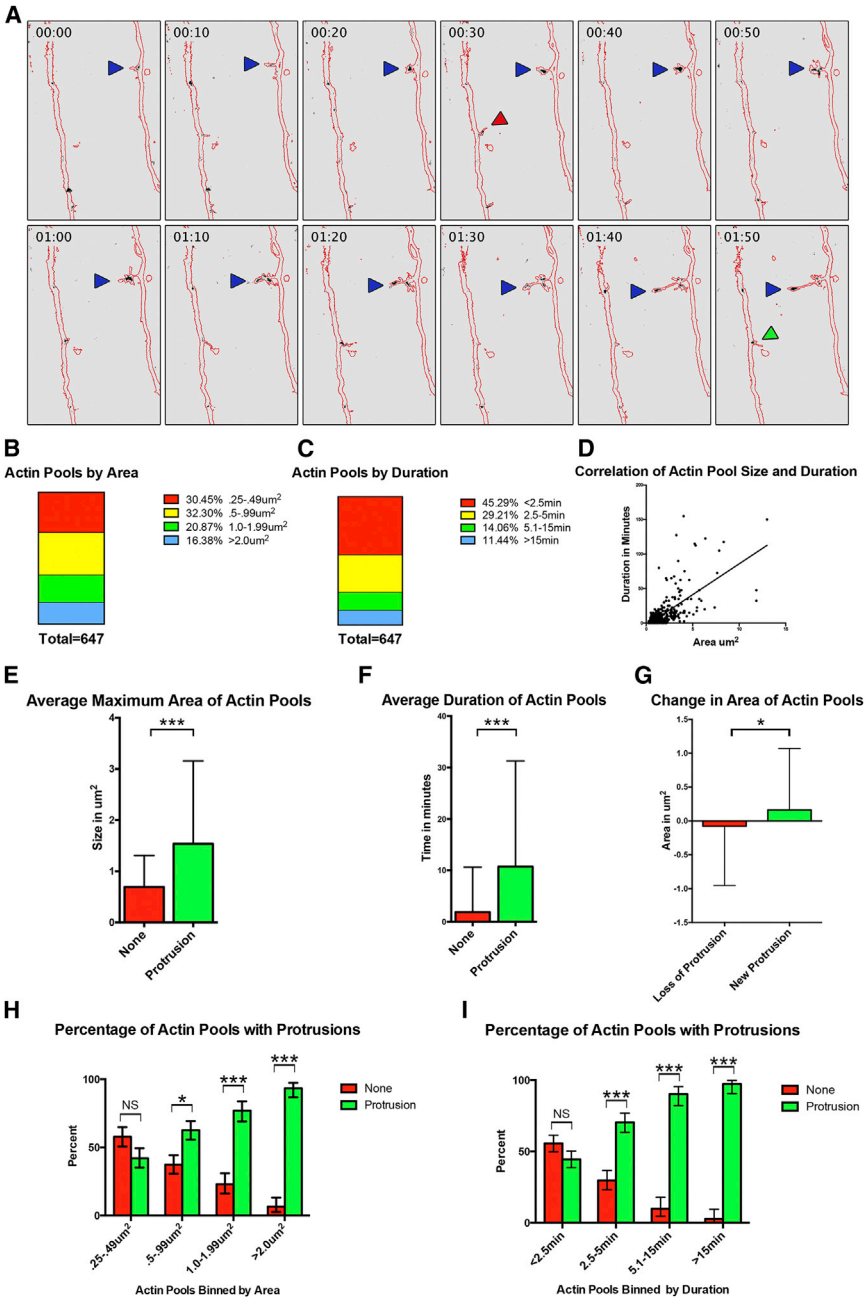

Figure 4. F-Actin Dynamics during Collateral Axon Branch Formation

(A) Time-lapse images of layer II/III pyramidal neuron axon co-labeled with eGFP and the calponin homology domain of utrophin fused to mRFP, an f-actin biosensor. Images were acquired every 2.5 min. Representative images are displayed every 10 min. The eGFP signal was used to create a mask of the axon (red outline), and the mRFP signal corresponding to f-actin is black (see also Movie S5). Blue arrows denote a newly formed collateral axon branch, the green arrow marks a newly formed protrusion emerging from the primary axon, and a red arrow marks a protrusion that is lost.

(B and C) The 647 f-actin pools quantified were binned by size (B) and by duration (C).

(D) A significant correlation was found between the size of the f-actin pool and the duration of the f-actin pool (p value < 0.0001).

(E and F) We compared the average area and duration of f-actin pools associated with a protrusion (green) and f-actin pools that did not correspond with a protrusion (red; E and F, respectively).

(G) If a protrusion was lost, there was a decrease in the size of the f-actin pool (red). If a new protrusion was formed from a pre-existing f-actin pool, there was an increase in the size of the f-actin pool (green).

(H) When the f-actin pools were binned by size, there was a significant increase in the percentage of f-actin pools corresponding with protrusions only in f-actin pools greater than 0.5 μm^2.

(I) When the f-actin pools were binned by duration, there was a significant increase in the percentage of f-actin pools corresponding with protrusions only in f-actin pools that persisted longer than 2.5 min.

* indicates a p value < 0.05. *** indicates a p value < 0.001. NS indicates no significance. Error bars denote SD (E–G) and 95% confidence intervals (H and I). See also Movie S5.

Extrinsic Signaling and the Regulation of Laminar-Specific Innervation Patterns

Laminar-specific innervation organizes a wide range of neural circuits throughout the nervous system, and molecular mechanisms underlying laminar organization are likely conserved. Within the mammalian retina, cell adhesion molecules including Sidekicks, DSCAMs, and cadherins regulate laminar-specific innervation of sublaminae within the inner plexiform layer (IPL) by neurites from amacrine, bipolar, and retinal ganglion cells (Duan et al., 2014; Yamagata and Sanes, 2008). Short-range repulsive cues, including semaphorin 5A (Sema5A), Sema5B, and Sema6A, also regulate laminar-specific innervation of amacrine, bipolar, and RGCs in the IPL and horizontal cells within the outer plexiform layer (OPL) (Matsuoka et al., 2011a,b, 2012; Sun et al., 2013). Taken together, these results show that cell adhesion molecules and repulsive guidance cues together contribute to laminar innervation of the retina, and it will be interesting to see whether similar mechanisms function in the cerebral cortex.

Intrinsic Signaling Mechanisms and Laminar-Specific Innervation Patterns

The formation of filopodia and lamellipodia provides initial steps in the elaboration of collateral axon branches, and this depends critically on actin cytoskeletal dynamics (Dent and Kalil, 2001; Kalil and Dent, 2014; this study). The activities of many actin regulatory proteins, including ARP2/3, cofilin, and Ena/VASP are

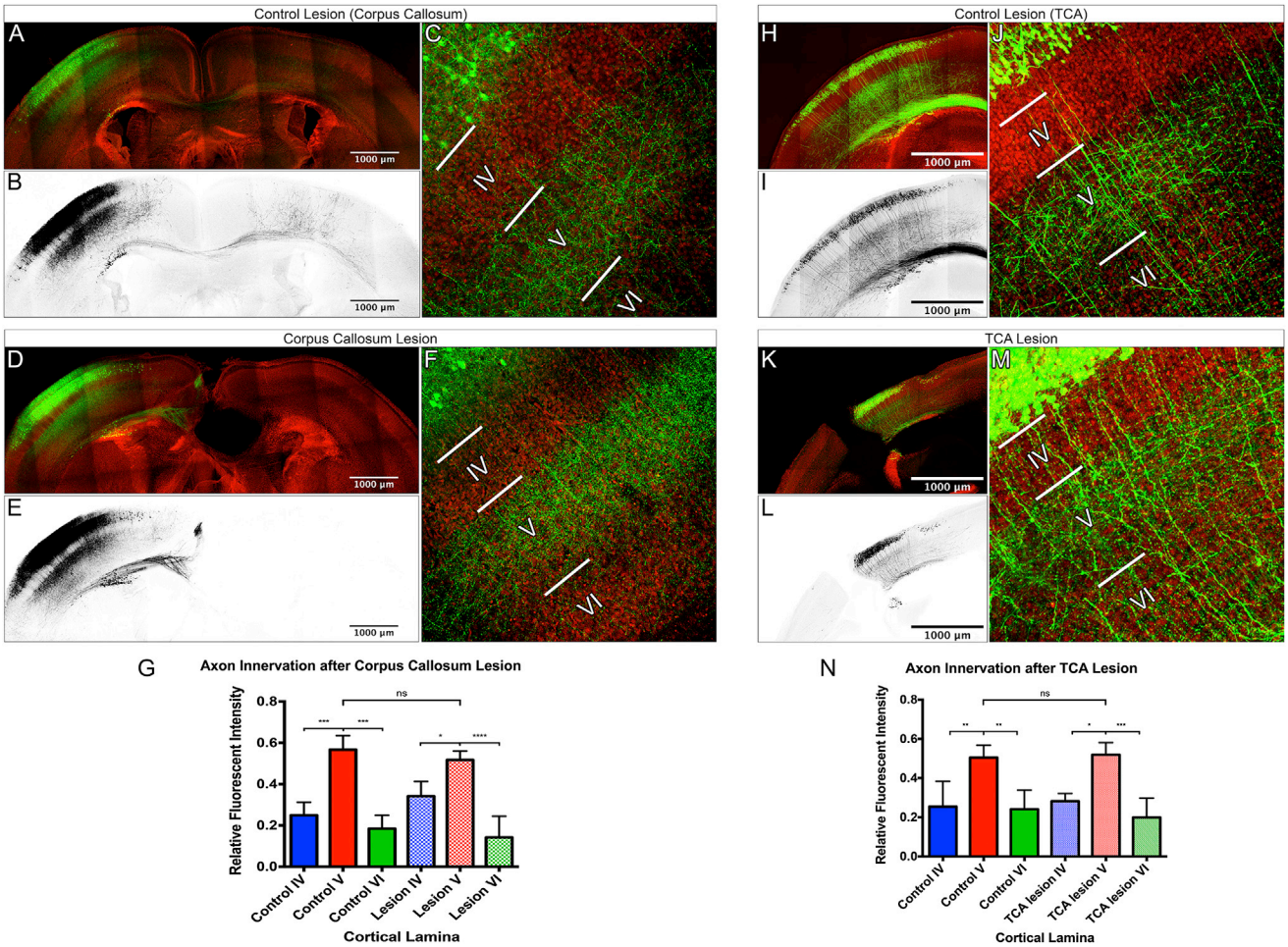

Figure 5. Midline Crossing, Callosal Axons, and Thalamocortical Axons Are Dispensable for Generating the Local Layer II/III Pyramidal Neuron Laminar-Specific Innervation Pattern

(A–F) Confocal images of 250-μm fixed coronal sections from P7 control brains (composite panoramic images: A and B; high magnification: C) or P7 brains in which the corpus callosum was lesioned at P0 (composite panoramic images: D and E; high magnification: F). Layer II/III pyramidal neurons were labeled by IUE with plasmids encoding eGFP (green: A, C, D, and F; black: B and E) and counter stained with DAPI (red: A, C, D, and F).

(G) Axon innervation was measured by relative eGFP fluorescence intensity within cortical layers. A significant increase in the innervation of layer V, as compared to layers IV and VI, was found in both control and lesioned animals, and this increase was not significantly different between control and lesioned animals.

(H–M) Confocal images of 250-μm fixed coronal sections from P5 control brains (composite panoramic images: H and I; high magnification: J) or P5 brains in which the thalamocortical axons (TCA) were lesioned at P0 (composite panoramic images: K and L; high magnification: M) are shown. S1 layer II/III pyramidal neurons were labeled by IUE with plasmids encoding tdTomato (green: H, J, K, and M; black: I and L) and counterstained with DAPI (red: H, J, K, and M). Axon innervation was measured by relative tdTomato fluorescence intensity within cortical layers in control animals (H–J) and animals with TCA lesions (K–M).

(N) A significant increase in the innervation of layer V, as compared to layers IV and VI, was found in both control and lesioned animals, and this was not different between control and lesioned animals. An ANOVA followed by a Tukey's test was used to compare innervation within groups (control or lesion), and a two-way ANOVA was used to compare means between groups (control versus lesion).

* indicates a p value < 0.05. *** indicates a p value < 0.001. **** indicates a p value < 0.0001. NS indicates no significance. Error bars denote SD. See also Figure S3.

coordinated with signaling molecules that include Rho family GTPases, CDC42, and Rac to regulate this process. Therefore, dynamic regulation of these signaling pathways likely underlies the filopodial and lamellipodial dynamics we observe in our time-lapse imaging. However, our determination that the rate of filopodium and lamellipodium formation in a given cortical layer does not correlate with the formation of stable collateral branches suggests that additional signaling mechanisms preferentially stabilize the cytoskeleton to form a collateral axon branch from a small protrusion. One signaling cascade that could serve to stabilize an axon collateral branch includes LKB1 and its downstream kinases Nuak1/2, because these kinases are key modulators of axon branching in cortical neurons (Courchet et al., 2013). Whereas molecular mechanisms regulating laminar-specific innervation within the cerebral cortex remain to be defined, it is likely that distinct signaling events are coordinated to form stable collateral axon branches within a given cortical layer.

Intrinsic neural activity shapes many neural circuits and is important for layer II/III pyramidal neuron axon branching in the contralateral cortex (Mizuno et al., 2010; Wang et al., 2007). However, we find that hyperpolarization did not alter the overall initiation of ipsilateral collateral branch formation, nor did it abolish local laminar-specific innervation. Recent work demonstrates that balanced inter-hemispheric neural activity is necessary for proper targeted innervation of the contralateral hemisphere by layer II/III pyramidal neurons (Suárez et al., 2014). Our observations employing lesions and Kir2.1 gain of function suggest that balanced inter-hemispheric activity is dispensable for local innervation of the ipsilateral S1 by layer II/III pyramidal neurons axon collateral branches. This raises the interesting possibility that collateral axon branches utilize unique molecular mechanisms to innervate their local environment within the ipsilateral S1 and that this microcircuitry of the cerebral cortex is genetically hardwired.

EXPERIMENTAL PROCEDURES

Targeted IUEs

Timed pregnant embryonic day 15.5 CD1 females were deeply anesthetized with either 2,2,2 tribromoethanol 2.5% in PBS (pH 7.4) or isoflurane. The incision site was shaved, cleaned, a small longitudinal incision (1.5–2 cm) was made, and the embryos removed and rinsed with sterile PBS. The lateral ventricles were injected with small volumes of DNA solutions in PBS (pH 7.4) with fast green dye. Embryos were electroplated with gene paddles (Harvard Apparatus) using a BTX square pulse electroporator: 30–40 V, 3 × 50-ms pulses with a 950-ms interval. The positive electrode was carefully placed above the differentiating areas of the primary somatosensory cortex. After electroporation, the embryos were placed back within the dam and the incision was sutured and stapled. The dam was returned to a heated cage and allowed to recover for several hours. All procedures were conducted in accordance to IUCAC-approved protocols. Plasmids used for IUE in this study are described in the Supplemental Experimental Procedures.

Immunostaining

Mice were deeply anesthetized and perfused with ice-cold PBS (pH 7.4) followed by 4% paraformaldehyde, PBS (pH 7.4). Brains were promptly dissected and post-fixed in 4% paraformaldehyde, PBS (pH 7.4) for 2 hr on ice. Fixed brains were washed in PBS, and either 250-μm coronal sections were prepared using a vibratome or 25-μm coronal sections were prepared using a cryostat. Brain sections were permeabilized and blocked in permeabilization buffer (3% BSA, 0.3% Triton X-100, and PBS [pH 7.4]) with rocking overnight at 4°C. Primary antibodies were diluted in permeabilization buffer and secondary antibodies were diluted in permeabilization buffer with 5% goat serum. The brain sections were incubated with antibody solutions overnight rocking at 4°C. After antibody incubations, brain sections were washed in PBS (pH 7.4) five times for 30 min with shaking at room temperature. Prior to imaging, floating brain sections were mounted onto glass slides and dried. Fluoro Gel with DABCO (Electron Microscopy Sciences) was applied to each slide and a coverslip mounted on top. A full list of antibodies used, including concentrations and catalog numbers, may be found in the Supplemental Experimental Procedures.

Live Imaging

Mouse pups were sacrificed at ages ranging from postnatal day 2 to 4. Brains were quickly removed and placed in sucrose solution (NaCl 83 mM, KCl 2.5 mM, $MgSO_4$ 3.3 mM, NaH_2PO_4 1 mM, $NaHCO_3$ 26.2 mM, D-glucose 22 mM, sucrose 72 mM, and $CaCl_2$ 0.5 mM [pH 7.4]) on ice while being continuously superfused with carbogen (95% O_2 and 5% CO_2). Brains were subsequently sectioned using a vibratome while in sucrose solution superfused with carbogen. The sections were 400 μm in depth and tilted slightly dorsally to the coronal plane to ensure the sections were perpendicular to the somatosensory cortex. Brain sections were embedded in 1 mg/ml collagen in the open perfusion configuration of the PECON POC-R2 cell cultivation system. After the collagen gel had solidified for 10 min at 37°C, brain sections were continually perfused with aCSF (NaCl 124 mM, KCl 2.5 mM, $MgCl_2$ 1.0 mM, NaH_2PO4 1.25 mM, $CaCl_2$ 2.5 mM, $NaHCO_3$ 26.2 mM, and D-glucose 25 mM [pH 7.4]) superfused with carbogen at a rate of 5 ml/min. Brain sections were allowed to recover for a minimum of 2 hr prior to the imaging session. A full description of microscopy, image processing, and data analysis may be found in the Supplemental Experimental Procedures.

Lesions and Viral Injections

All lesions and viral injections were performed on deeply anesthetized P0 mice on ice. Bupivacaine was administered prior to making a small incision through the skin overlying the skull. For viral injections, a small incision through the skull was made to allow passage of a Hamilton syringe. One hundred nanoliters of high-titer AAV-encoding GFP was injected at approximately +0.070 cm bregma, +0.096 cm lateral, and at a depth of 2 mm. All lesions were performed with a microscalpel. After the procedure, the incision was closed and mice were allowed to recover on a warming pad before being returned to their cage.

SUPPLEMENTAL INFORMATION

Supplemental Information includes Supplemental Experimental Procedures, four figures, one table, and five movies and can be found with this article online at http://dx.doi.org/10.1016/j.celrep.2015.06.026.

AUTHOR CONTRIBUTIONS

R.A.H. and A.L.K. are responsible for the conception and design of the study. R.A.H., S.K., and E.T. performed all experiments. R.A.H. and A.L.K. analyzed the data, drafted, and wrote the article. As senior author, A.L.K. supervised all aspects of this study.

ACKNOWLEDGMENTS

We thank Dr. Alain Chédotal for helpful suggestions on using the MAGIC marker approach and for generously sharing the pCx-Cytobow plasmid; Drs. Brendan Lilley, Martín Riccomagno, Kevin Wright, and Fengquan Zhou for helpful comments and suggestions on the manuscript; and members of the A.L.K. laboratory for assistance. A.L.K. is an investigator of the Howard Hughes Medical Institute.

Received: February 5, 2015
Revised: April 18, 2015
Accepted: June 5, 2015
Published: July 2, 2015

REFERENCES

Akers, R.M., and Killackey, H.P. (1978). Organization of corticocortical connections in the parietal cortex of the rat. J. Comp. Neurol. *181*, 513–537.

Bortone, D., and Polleux, F. (2009). KCC2 expression promotes the termination of cortical interneuron migration in a voltage-sensitive calcium-dependent manner. Neuron *62*, 53–71.

Burkel, B.M., von Dassow, G., and Bement, W.M. (2007). Versatile fluorescent probes for actin filaments based on the actin-binding domain of utrophin. Cell Motil. Cytoskeleton *64*, 822–832.

Courchet, J., Lewis, T.L., Jr., Lee, S., Courchet, V., Liou, D.Y., Aizawa, S., and Polleux, F. (2013). Terminal axon branching is regulated by the LKB1-NUAK1 kinase pathway via presynaptic mitochondrial capture. Cell *153*, 1510–1525.

De Marco García, N.V., Karayannis, T., and Fishell, G. (2011). Neuronal activity is required for the development of specific cortical interneuron subtypes. Nature *472*, 351–355.

Dent, E.W., and Kalil, K. (2001). Axon branching requires interactions between dynamic microtubules and actin filaments. J. Neurosci. *21*, 9757–9769.

Dent, E.W., Callaway, J.L., Szebenyi, G., Baas, P.W., and Kalil, K. (1999). Reorganization and movement of microtubules in axonal growth cones and developing interstitial branches. J. Neurosci. *19*, 8894–8908.

Duan, X., Krishnaswamy, A., De la Huerta, I., and Sanes, J.R. (2014). Type II cadherins guide assembly of a direction-selective retinal circuit. Cell *158*, 793–807.

Fame, R.M., MacDonald, J.L., and Macklis, J.D. (2011). Development, specification, and diversity of callosal projection neurons. Trends Neurosci. *34*, 41–50.

Gibson, D.A., and Ma, L. (2011). Developmental regulation of axon branching in the vertebrate nervous system. Development *138*, 183–195.

Hand, R., and Polleux, F. (2011). Neurogenin2 regulates the initial axon guidance of cortical pyramidal neurons projecting medially to the corpus callosum. Neural Dev. *6*, 30.

Hatanaka, Y., and Yamauchi, K. (2013). Excitatory cortical neurons with multipolar shape establish neuronal polarity by forming a tangentially oriented axon in the intermediate zone. Cereb. Cortex *23*, 105–113.

Johns, D.C., Marx, R., Mains, R.E., O'Rourke, B., and Marbán, E. (1999). Inducible genetic suppression of neuronal excitability. J. Neurosci. *19*, 1691–1697.

Kalil, K., and Dent, E.W. (2014). Branch management: mechanisms of axon branching in the developing vertebrate CNS. Nat. Rev. Neurosci. *15*, 7–18.

Loulier, K., Barry, R., Mahou, P., Le Franc, Y., Supatto, W., Matho, K.S., Ieng, S., Fouquet, S., Dupin, E., Benosman, R., et al. (2014). Multiplex cell and lineage tracking with combinatorial labels. Neuron *81*, 505–520.

Matsuoka, R.L., Chivatakarn, O., Badea, T.C., Samuels, I.S., Cahill, H., Katayama, K., Kumar, S.R., Suto, F., Chédotal, A., Peachey, N.S., et al. (2011a). Class 5 transmembrane semaphorins control selective Mammalian retinal lamination and function. Neuron *71*, 460–473.

Matsuoka, R.L., Nguyen-Ba-Charvet, K.T., Parray, A., Badea, T.C., Chédotal, A., and Kolodkin, A.L. (2011b). Transmembrane semaphorin signalling controls laminar stratification in the mammalian retina. Nature *470*, 259–263.

Matsuoka, R.L., Jiang, Z., Samuels, I.S., Nguyen-Ba-Charvet, K.T., Sun, L.O., Peachey, N.S., Chédotal, A., Yau, K.W., and Kolodkin, A.L. (2012). Guidance-cue control of horizontal cell morphology, lamination, and synapse formation in the mammalian outer retina. J. Neurosci. *32*, 6859–6868.

Mizuno, H., Hirano, T., and Tagawa, Y. (2007). Evidence for activity-dependent cortical wiring: formation of interhemispheric connections in neonatal mouse visual cortex requires projection neuron activity. J. Neurosci. *27*, 6760–6770.

Mizuno, H., Hirano, T., and Tagawa, Y. (2010). Pre-synaptic and post-synaptic neuronal activity supports the axon development of callosal projection neurons during different post-natal periods in the mouse cerebral cortex. Eur. J. Neurosci. *31*, 410–424.

Price, D.J., Kennedy, H., Dehay, C., Zhou, L., Mercier, M., Jossin, Y., Goffinet, A.M., Tissir, F., Blakey, D., and Molnár, Z. (2006). The development of cortical connections. Eur. J. Neurosci. *23*, 910–920.

Suárez, R., Fenlon, L.R., Marek, R., Avitan, L., Sah, P., Goodhill, G.J., and Richards, L.J. (2014). Balanced interhemispheric cortical activity is required for correct targeting of the corpus callosum. Neuron *82*, 1289–1298.

Sun, L.O., Jiang, Z., Rivlin-Etzion, M., Hand, R., Brady, C.M., Matsuoka, R.L., Yau, K.W., Feller, M.B., and Kolodkin, A.L. (2013). On and off retinal circuit assembly by divergent molecular mechanisms. Science *342*, 1241974.

Wang, C.-L., Zhang, L., Zhou, Y., Zhou, J., Yang, X.-J., Duan, S., Xiong, Z.-Q., and Ding, Y.-Q. (2007). Activity-dependent development of callosal projections in the somatosensory cortex. J. Neurosci. *27*, 11334–11342.

Yamagata, M., and Sanes, J.R. (2008). Dscam and Sidekick proteins direct lamina-specific synaptic connections in vertebrate retina. Nature *451*, 465–469.

Yu, C.R., Power, J., Barnea, G., O'Donnell, S., Brown, H.E., Osborne, J., Axel, R., and Gogos, J.A. (2004). Spontaneous neural activity is required for the establishment and maintenance of the olfactory sensory map. Neuron *42*, 553–566.